Atmospheric Feedbacks over the Tropical Pacific in Observations and Atmospheric General Circulation Models: An Extended Assessment

Chunqiang Wu [1,2], Tianjun Zhou [1], De-Zheng Sun [3]

1 LASG, Institute of Atmospheric Physics, Chinese Academy of Sciences, Beijing 100029, China

2 Graduate School of Chinese Academy of Sciences

3 Cooperative Institute for Environmental Studies/University of Colorado & NOAA/Earth System Research Laboratory, Boulder, Colorado, USA.

(Submitted to Journal of Climate)

Corresponding author:

Chunqiang Wu

LASG, Institute of Atmospheric Physics

Chinese Academy of Sciences

Beijing 100029, China.

Fax: 86-10-8299-5172

Email: wucq@mail.iap.ac.cn

Abstract

The dynamical and radiative feedbacks from the deep convection over the tropical Pacific are quantified using ENSO signal in that region for both the observation and 16 climate models. Different from a previous analysis, we recognize the nonlinear relationship between deep convection and SST over that region, and perform the evaluation using the data from the warm phase and the cold phase separately. We also employ a much longer dataset than the previous analysis. While the results confirm the previous finding that most models underestimate the cloud albedo feedback and overestimate the water vapor feedback, we also show that the discrepancies mainly come from the warm phase, underscoring deep convection as a major source of error. In the cold phase, the models are found to have feedbacks of comparable magnitude and similar spatial pattern to the observations. Examination of the cause of the weaker feedback from cloud albedo in the models suggests that the bias is likely linked to a weaker relationship between the short-wave cloud forcing and the precipitation in the models. In addition, the analysis reveals a systematic feedback bias from the latent heat flux: the models tend to have a too strong positive feedback of latent heat flux over the central Pacific. The results suggest that the deficiency in the atmospheric feedbacks, particularly those from the deep convection, is a possible cause for the excessive cold-tongue in coupled models.

1. Introduction

The equatorial Pacific cold-tongue plays a fundamental role in the heat and carbon balance of the coupled ocean-atmosphere system (Sun 2003, Feely et al. 1999). The processes and feedbacks that control the cold tongue are not well understood and the current non-flux adjust coupled general circulation models (CGCMs) do not properly simulate it (Mechoso et al. 1995; Latif et al. 2001; Davey et al. 2002). The CGCMs suffer from an extensive cold-tongue issue: the simulated equatorial cold tongue is typically too strong, too narrow, and extends too far to the west. The bias in the cold tongue may negatively impact the model-simulated variability on various temporal-spatial scales (Wittenberg et al. 2006; Large and Danabasoglu 2006), as these variabilities may depend on the mean state of coupled tropical Pacific ocean-atmosphere. So, it is imperative to eliminate this bias from climate models.

The extensive cold tongue problem is a long-standing tropical bias in the CGCMs. The early hypotheses attribute this problem to the errors or incomplete representation of the involved processes in the individual components of the coupled model. For example, Murtugudde et al. (2002) and Lin et al. (2008) suggested that the lack of phytoplankton in the model ocean could lead to an underestimate of the solar radiation absorbed by the ocean. Stockdale et al. (1998) and Wu et al. (2005) pointed out that the lack of sufficient vertical resolution of the ocean model is a possible cause to this bias because such a deficiency may cause an excessive cooling of the surface ocean. In the same vein, the winds are not perfect in the atmospheric models and these

errors may induce excessive equatorial upwelling upon coupling. The surface heating from the atmospheric general circulation model (AGCM) may also be too weak, even with the observed SST (Sun et al. 2003). However, the mean state depends critically on the internal feedback processes that amplify or dampen the influence of initial errors in models. So, why does significant systematic bias exist in the tropical region, where there are known strong negative feedbacks (Ramanathan and Collins 1991; Wallace 1992, Sun and Trenberth 1998)? Sun et al (2003) and Sun et al (2006) hypothesized that the tendency for the CGCMs to develop an excessive cold-tongue in the equatorial Pacific is at least in part due to a weak regulating effect from the deep convection on SST changes in that region. The corresponding weaker constraining effect on the SST change by the surface heating then results in an "over-expression" of the effect of ocean dynamics, leading to the development of an excessive cold-tongue in the coupled model. Sun et al. (2003) and Sun et al. (2006) used the radiative fluxes at the Top of the Atmosphere (TOA) to assess the radiative feedbacks from water vapor and clouds. Lin (2007) echoed the same concern with a feedback analysis focused on the surface level.

In the studies of Sun et al. (2003) and Sun et al (2006), the ERBE satellite data (Barkstrom 1984), which covers the period from 1985 to 1989, is used to estimate the radiative and dynamic feedbacks. However, since the ERBE data essentially covers only one ENSO cycle, the estimate based on such a short dataset may limit the robustness of the conclusion from the analysis. In addition, considering differences in magnitude and spatial pattern among the different ENSO events (Wang and Fiedler

2006; Weng et al. 2007) as well as the potential dependence of the involved radiative processes on these differences (Cess et al. 2001; Allan et al. 2002; Lu et al. 2004), we extend the analysis to a longer period to see whether the results still holds. Perhaps, more importantly, the works of Sun et al. (2003) and Sun et al. (2006) did not exclude the La Niña episodes. Considering the strongly nonlinear relationship exists in the convective activities for different phases of the SST anomaly (SSTA) in the eastern equatorial Pacific, a negative SSTA has no further effect on the convection-related feedbacks (Hoerling et al. 1997) and the inclusion of La Niña episodes may underestimate the feedbacks from deep convection. Note that it is the feedbacks from deep convection that Sun et al. (2003) and Sun et al. (2006) intended to assess. Theoretically, the western Pacific warm pool is the most appropriate region for assessing the feedbacks from deep convection, but the SST variability over that region is too small to quantify the feedbacks from deep convection. So we still focus the analysis of the atmospheric feedbacks on the region of the tropical Pacific — the feedbacks over the equatorial Pacific cold tongue region, which provides a sufficiently large signal in the SST field. However, we use a longer data set, and for the reasons just stated, estimate the feedbacks for the cold and warm phase separately. We note that precluding the cold phase data in the regression analysis is equivalent to taking the average temperature in the warm phase as the reference temperature in estimating the feedbacks from deep convection, and therefore the results should be more an accurate assessment of the feedbacks from deep convection. Indeed, as we will show, the model-observation discrepancy in the net surface heat flux feedback

obtained this way is particularly more apparent compared to that obtained from both phases of ENSO.

The rest of this paper is organized as follows. Descriptions of the methodology, models and observational data are presented in section 2. In section 3, we show the results based on data over a longer period, which covers three ENSO cycles. In section 4, we explore the feedbacks in the cold and warm phases separately. The feedback from the latent heat flux is examined in section 5. Finally, a summary is given in section 6.

2. Methodology, model descriptions and observational data

As in Sun et al. (2003) and Sun et al. (2006), we use the response of tropical convection to ENSO forcing to obtain the feedbacks of water vapor and clouds associated with convection. In this study, we take the SSTA averaged over the entire Pacific cold-tongue region (5^oS-5^oN, 150^oE-110^oW) as a forcing signal, then explore how radiative fluxes at TOA, vertically integrated atmospheric energy transport and surface turbulent heat fluxes response to the underlying SSTA by linear regression analysis.

Some crucial components involved in this analysis are described as follow: The clear-sky greenhouse effect (Ga) at TOA is quantified as Raval and Ramanathan (1989),

$$Ga = \sigma T_s^4 - LW_{clear} \qquad (1)$$

Following Charlock and Ramanathan (1985), the longwave (Cl) and shortwave (Cs) cloud radiative forcings at TOA are defined as

$$Cl = LW_{clear} - LW \qquad (2)$$
$$Cs = SW - SW_{clear} \qquad (3)$$

In the above equations, σ is the Stefan-Boltzmann constant; Ts denotes SST. We assume the surface emissivity to be unity since only ocean regions are concerned in this study. LW_{clear} and LW represent the upward clear-sky and full-sky long-wave flux at TOA, respectively. SW_{clear} and SW are the clear-sky and full-sky net downward solar radiation flux at TOA separately. The net surface heat flux (Fs) is the sum of net downward shortwave and longwave radiation at surface and the turbulent fluxes. The atmospheric energy transport (Da) is calculated as the difference between the Fs and the net radiative flux at TOA. The definition of feedback symbols and the procedure of calculation are the same as in Sun et al. (2003) and Sun et al. (2006). Neglecting the heat storage in the atmosphere, which is small (Sun 2000), the net surface heat flux feedback $\partial Fs/\partial T$ differs from total atmosphere feedback ($\partial Ga/\partial T + \partial Cl/\partial T + \partial Cs/\partial T + \partial Da/\partial T$) by a constant — the rate of change of the ocean's surface emission with respect to SST. So, $\partial Fs/\partial T = \partial Ga/\partial T + \partial Cl/\partial T + \partial Cs/\partial T + \partial Da/\partial T +$ Const.

There are 16 AGCMs used in this study. Twelve of these models are derived from the World Climate Research Programme's (WCRP's) Coupled Model Inter-comparison Project phase 3 (CMIP 3) multi-model dataset. The other 4 models are similar to those used in Sun et al (2006). Table 1 shows a brief summary of the

analyzed models. In this study, we focus on evaluating the model outputs covering 1985-1999. Note that some AGCMs in Atmospheric Model Inter-comparison Project phase II (AMIP II) experiments do not have specific names. For brevity, we use the names of coupled models to represent these models in the following discussion. Readers are referred to Sun et al. (2006) and the website of the U.S. Department of Energy's Program for Climate Model Diagnosis and Inter-comparison (PCMDI) for more information (see http://www-pcmdi.llnl.gov/ipcc/about_ipcc.php).

The observational data sets used to verify models are summarized as follows: 1) Radiative fluxes at TOA as well as surface from the International Satellite Cloud Climatology Project (ISCCP) flux D (FD) monthly mean data (Zhang et al. 2004), which holds an overall uncertainties of 5–10 Wm^{-2} at TOA and of 10–15 Wm^{-2} at the surface; 2) The latent and sensible heat fluxes from OAFlux (Objective Analyzed Air–Sea Fluxes) (Yu and Weller, 2007). The flux-related basic surface meteorological variables are obtained through synthesizing satellite data and outputs of numerical weather prediction. The surface net heat flux and Da are calculated by combining ISCCP FD and OAFlux. Yu et al. (2006) argued that this combination is superior to the numerical weather reanalysis. 3) The heat fluxes at TOA and surface from NCEP/NCAR reanalysis (Kistler et al. 2001), which is not synthesized by OAFlux; 4) The SST from the Extended Reconstruction SST (ERSST v2) data set (Smith and Reynolds 2004).

3. Feedbacks assessed over a longer period

The time series of SSTA averaged over the Pacific cold-tongue region, on which the variabilities are regressed, are presented in Fig. 1. This time series covers 3 ENSO cycles which allow us to obtain more representative results. More importantly, the longer data give us an opportunity to estimate the feedbacks in the cold and warm phases separately. As shown in Fig. 1, the mean of temperature anomaly (the reference temperature) for the warm phase is about 0.5^{o}C, while that for the cold phase is about -0.6^{o}C. The corresponding total SSTs are 28.3^{o}C and 27.1^{o}C respectively. During the warm phase, the area averaged total SSTs are above 27.5 ^{o}C and most of them exceed 28 ^{o}C. However, during the cold phase, the total SSTs are below 28 ^{o}C. It indicates that choosing the data during the warm phase to estimate the feedbacks from the deep convection is more appropriate, as deep convection generally does not take place below 27 ^{o}C (Ramanathan and Collins1991, Sud et al. 1999)

Over the ERBE period, from 1985 to 1989, the feedbacks estimated from ISCCP and ERBE are consistent. The feedbacks of ∂Ga/∂T, ∂Cl/∂T and ∂Cs/∂T in ISCCP are 6.35, 12.64 and -12.34 $Wm^{-2}K^{-1}$ respectively. Comparison between these feedbacks with those in Table 1 of Sun et al. (2006) indicates that the estimate of ∂Ga/∂T and ∂Cl/∂T feedbacks in two datasets are comparable; For the ∂Cs/∂T feedback, the difference is also within the range of uncertainty. For the ∂Da/∂T (∂Fs/∂T) feedback, the estimate from a combination of ISCCP and OAFlux is -17.71(-17.31) $Wm^{-2}K^{-1}$, which is close to the estimate from the European Centre for Medium-Range Weather Forecasts (ECMWF) 40-year reanalysis (Uppala et al. 2005, hereafter ERA40) in Table 1 of Sun et al. (2006). This agreement adds confidence in extending our

analysis to a longer time period and to estimate the feedbacks in the cold and warm phases separately.

Using the same technique as in Sun et al. (2006), the feedbacks over the Pacific cold-tongue region during a much longer period (1985-1999) are calculated and listed in Table 2. The $\partial Fs/\partial T$ and $\partial Da/\partial T$ feedback in parenthesis are the results from the NCEP/NCAR reanalysis. Those from the ERA40 are comparable to those from NCEP/NCAR reanalysis (not shown).

On the ENSO time scale, in the observation, the $\partial Fs/\partial T$ feedback averaged over the Pacific cold-tongue region is about $-21.51 Wm^{-2}K^{-1}$ (Table 2) which is a strong damper to the SST change. All models underestimate this feedback except for the MPI ECHAM5 model. These results confirm the suspicion that the underestimate of regulatory effect from the atmosphere on the underlying SST over the Pacific cold-tongue region is a prevalent problem in climate models. In Sun et al (2006), two GFDL models have comparable $\partial Fs/\partial T$ feedback to the observation, although both of their corresponding coupled models suffer from an extensive cold-tongue. Our analysis based on a much longer data set indicates that these two models still bear insufficient $\partial Fs/\partial T$ feedback. The $\partial Fs/\partial T$ feedbacks from the two GFDL models are less than $-15 Wm^{-2}K^{-1}$, and these two models have positive biases larger than $6.0 Wm^{-2}K^{-1}$. With the exception of MPI ECHAM5, the positive bias in the $\partial Fs/\partial T$ feedback ranges from $22.31 Wm^{-2}K^{-1}$ in NCAR CAM2 to $3.98 Wm^{-2}K^{-1}$ in MRI CGCM. If we take the result from the NCEP/NCAR reanalysis as the reference to compare with, there are 4 models (CCSR MIROC_M, MRI CGCM, MPI ECHAM5

and UKMO HadGAM1) having comparable or even excessive ∂Fs/∂T feedback. It is known, however, that the surface heat flux data from the NCEP/NCAR reanalysis is less reliable, because it depends heavily on the model physics (which is what we attempt to evaluate here).

The geographical patterns of the ∂Fs/∂T feedback are presented in Fig. 2. In the observation, the negative ∂Fs/∂T feedback exhibits a zonally elongated structure over the equator, extending from about 150°E to 110°W, with a center over the eastern equatorial Pacific which exceeds -40$Wm^{-2}K^{-1}$. Compared to the observations, two discrepancies stand out: i) All models have a positive bias over the central-western equatorial Pacific. Moreover, the positive bias along the equator in some models (NCAR CAM2, NCAR CAM3T42, NCAR CAM3T85, NASA NSIPP1 and CNRM CM3) extends to the date line. ii) Most models have insufficient negative ∂Fs/∂T feedbacks over the far eastern equatorial Pacific, in particular IAP GAMIL1 and IPSL LMDZ4.

The negative ∂Fs/∂T feedbacks in most models are insufficient. Furthermore, Table 2 shows that the bias is mainly due to the underestimate of negative feedbacks from cloud albedo (∂Cs/∂T) and atmospheric transport (∂Da/∂T), and to a less degree due to the overestimate of positive feedback from greenhouse effect of water vapor and clouds.

The ∂Cs/∂T feedback is the largest uncertainty in radiative feedbacks. The observed ∂Cs/∂T feedback is about -13.98 $Wm^{-2}K^{-1}$, while those in models range from

2.43$Wm^{-2}K^{-1}$ in NCAR CAM2 to -19.90$Wm^{-2}K^{-1}$ in MPI ECHAM5. The positive $\partial Cs/\partial T$ feedback in NCAR CAM2 implies that the radiative process is distorted in this model. Table 2 shows that not all models underestimate the $\partial Cs/\partial T$ feedback. Among these 16 models, there are 7 models (GFDL AM2p10, GFDL AM2p12, UKMO HadGAM1, IPSL LMDZ4, MPI ECHAM5, CNRM CM3 and INM CM3) having comparable or even excessive $\partial Cs/\partial T$ feedback. However, the magnitude of the underestimate of $\partial Cs/\partial T$ feedback is larger than that of the overestimate. For example, among 9 models that underestimate the $\partial Cs/\partial T$ feedback, 6 models have biases around -10$Wm^{-2}K^{-1}$; however, among 7 models that have comparable feedback, 5 models have biases less than 3$Wm^{-2}K^{-1}$.

The spatial patterns of $\partial Cs/\partial T$ feedback are shown in Fig. 3. In the observations, the negative $\partial Cs/\partial T$ feedback centers in the central equatorial Pacific and extends to the far eastern equatorial Pacific. The spatial patterns of $\partial Cs/\partial T$ feedback in the models differ from each other. Most models (9 out of 16 models) can reproduce the negative $\partial Cs/\partial T$ feedback in the central equatorial Pacific with comparable values, while others show insufficient $\partial Cs/\partial T$ feedback there. The insufficient $\partial Cs/\partial T$ feedbacks are obvious in two NCAR models (NCAR CAM32 and NCAR CAM3T42) and two CCSR models (CCSR MIROC_M and CCSR MIROC_H). In addition, all models have a positive $\partial Cs/\partial T$ feedback bias over the far eastern equatorial Pacific. In particular in MRI CGCM3, NASA NSIPP1 and IPSL LMDZ4, their positive biases extend to the west of 150^{o}W.

Besides the $\partial Cs/\partial T$ feedback, the $\partial Da/\partial T$ feedback is another major source for

model climate sensitivity uncertainty: the spread of ∂Da/∂T feedback among the models is as large as that of ∂Cs/∂T which ranges from -10.13Wm^{-2}/K (CNRM ARPEGE3) to -28.73$Wm^{-2}K^{-1}$ (MRI CGCM), while the observed value is about -21.21 $Wm^{-2}K^{-1}$. More than half of the models (9 out of 16 models) underestimate the ∂Da/∂T feedback and most of them (8 out of 9 models) have a positive bias larger than 6$Wm^{-2}K^{-1}$. Meanwhile, there are 3 models having excessive ∂Da/∂T feedbacks — these biases are around 5$Wm^{-2}K^{-1}$. The spatial patterns of ∂Da/∂T feedback are also examined (not shown). In the observation, the ∂Da/∂T feedback shows a zonally elongated structure along the equator. Different from the simulations of ∂Cs/∂T feedback, all models have spatial patterns of ∂Da/∂T feedback similar to the observations. However, the positive bias over the central-western equatorial Pacific is obvious in all models.

Compared to the underestimate of ∂Cs/∂T and ∂Da/∂T feedbacks, the overestimate of the feedback from the greenhouse effect (including ∂Ga/∂T and ∂Cl/∂T) is secondary. The overestimate of ∂Ga/∂T and ∂Cl/∂T is dominant only in two models (GFDL AM2p12 and IPSL LMDZ4). While in these two models, the ∂Cs/∂T and ∂Da/∂T feedbacks are close to the observations. In addition, our results confirm the earlier finding that the ∂Ga/∂T feedback is overestimated in all models. Among these 16 AGCMs, only two models, i.e. CCSR MIROC_M and NASA GISS_ER, have ∂Ga/∂T feedbacks comparable to the observations; all other models have positive biases ranging from 1.8$Wm^{-2}K^{-1}$ (IAP GAMIL) to 3.8$Wm^{-2}K^{-1}$ (UKMO HadGAM1).

4. Feedbacks assessed using the data from the warm phase of ENSO only

In Sun et al. (2003) and Sun et al. (2006), the coupled tropical ocean-atmosphere system is approximated as a linear feedback system. However, as shown by Fig. 5 in Sun et al. (2008), the responses of precipitation and net surface solar radiation to SSTA over the central-eastern equatorial Pacific are nonlinear. So, could the inclusion of La Niña phase, during which the convection is suppressed, in estimating the feedbacks contaminate the hypothesis that the excessive cold-tongue issue is related to the weak regulating effect from the model atmosphere? To examine this possibility, the feedbacks are estimated for warm and cold phases separately. The results for the warm phase are summarized in Table 3. Also shown are the results from the NCEP/NCAR reanalysis.

The observed $\partial Fs/\partial T$ feedback is about -26.29$Wm^{-2}K^{-1}$ in the warm phase (Table 3). All models underestimate the $\partial Fs/\partial T$ feedback over the cold-tongue region (Table 3). The MPI ECHAM5, which has the strongest $\partial Fs/\partial T$ feedback (-21.90$Wm^{-2}K^{-1}$) among 16 models, still have significantly weaker $\partial Fs/\partial T$ feedback than the observation. All of the other models have positive bias larger than 10$Wm^{-2}K^{-1}$. In particular, there are 3 models (NCAR CAM2, NCAR CAM3T42 and IAP GAMIL) having positive $\partial Fs/\partial T$ feedback. Note that for coupled models that have an excessive cold-tongue problem (Lin 2007), their atmospheric components suffer from a same disease: a weak $\partial Fs/\partial T$ feedback in the warm phase. In the cold phase, the $\partial Fs/\partial T$ feedbacks in 5 models (i.e. GFDL AM2p10, CCSR MIROC_M, MRI CGCM, UKMO

HadGAM1 and MPI ECHAM5) are comparable to the observations. An interesting aspect of Table 3 is that, in the observations, the negative $\partial Fs/\partial T$ feedback in the warm phase is about $-5 Wm^{-2}K^{-1}$ stronger than that during the entire ENSO cycle. However, in all models with the exception of NCAR CAM3T85 and INM CM3, the $\partial Fs/\partial T$ feedbacks in the warm phase are weaker than that during the entire ENSO cycles. Among these models, the positive bias of $\partial Fs/\partial T$ feedback is larger than $5 Wm^{-2}K^{-1}$ in NCAR CAM2 and CNRM ARPEGE3.

To illustrate the differences between the $\partial Fs/\partial T$ feedbacks during the warm phase and that during the entire ENSO cycle, we show in Fig. 4 that the difference maps of $\partial Fs/\partial T$ feedbacks between these two estimates. In the observations, compared to the entire ENSO cycle, the negative $\partial Fs/\partial T$ feedback along the equator in the warm phase is enhanced to the east of the date line and is decreased to the west of it, indicating an eastward shift in the center of $\partial Fs/\partial T$ feedback. All models underestimate the enhancement of $\partial Fs/\partial T$ feedback over the central-eastern Pacific. For example, the $\partial Fs/\partial T$ feedbacks in the warm phase in three models (NCAR CAM2, IAP GAMIL1 and CNRM ARPEGE3) are smaller than that during the entire ENSO cycle in the central equatorial Pacific, even in the eastern tropical Pacific. Considering the dissimilarities in the spatial pattern of $\partial Fs/\partial T$ feedbacks during the entire ENSO cycle, it was expected that the difference maps of $\partial Fs/\partial T$ feedback between the warm phase and the entire ENSO cycle among the observation and the models differ from each other. It is thus particularly interesting to note that all models underestimate the enhancement of $\partial Fs/\partial T$ feedback over the central-eastern equatorial Pacific from

entire ENSO cycle condition to the warm phase condition. The latter is more relevant to deep convection, indicating that the bias in ∂Fs/∂T feedback is more closely related to the deep convection process in the models.

For most models, the underestimate of the nonlinearity of ∂Fs/∂T feedback, defined as the difference between the warm phase and the entire ENSO cycle, are primarily due to the insufficient nonlinearity of ∂Cs/∂T feedback, and to a less degree due to that in ∂Da/∂T feedback. In the observation, the ∂Cs/∂T feedback in the warm phase increases by about -9.6$Wm^{-2}K^{-1}$ compared to that during the entire ENSO cycles, signifying a strong nonlinear behavior. Although all models can capture the nonlinear behavior in the ∂Cs/∂T feedback, nearly all of them underestimate this nonlinearity except for INM CM3, which has an increase of -12.6$Wm^{-2}K^{-1}$. For example, the changes of the ∂Cs/∂T feedback in 10 models are within -5$Wm^{-2}K^{-1}$. The difference map of ∂Cs/∂T feedback between the warm phase and the entire ENSO cycles are presented in Fig. 5. In the observation, the negative ∂Cs/∂T feedback enhances over the equatorial Pacific to the east of date line which is manifested in the change of ∂Fs/∂T feedback. However, the majority of models underestimate the enhancement of this feedback.

Compared to that during the entire ENSO cycle, in the observations, the negative ∂Da/∂T feedback in the warm phase increases by about -1$Wm^{-2}K^{-1}$. This increase is within the range of estimate uncertainty. Interestingly, most of the models have a weaker ∂Da/∂T feedback in the warm phase relative to the entire ENSO cycle. In particular, three models (IAP GAMIL1, MRI CGCM and CNRM ARPEGE3), in

which the negative ∂Da/∂T feedback bias is larger than $5Wm^{-2}K^{-1}$. In general, the insufficient increase in negative ∂Cs/∂T feedback and the decrease in the negative ∂Da/∂T feedback in some models fail to cancel the increase in the positive feedback of ∂Ga/∂T and ∂Cl/∂T, although most models also underestimate the nonlinearity in these two positive feedbacks.

5. The feedback from the latent heat flux

The surface latent heat flux (LHF) in the tropical oceans is the second largest component in the energy budget at the surface. Moreover, the LHF-SST feedback has been suggested as an important process that modulates the tropical SST (Newell 1979; Zhang and McPhaden 1995). The amplitudes of LHF-SST feedbacks averaged over the Pacific cold-tongue region in the observation and models during the entire ENSO cycle are listed in Table 4. Also shown is the feedback from the sensible heat flux. The feedbacks from these turbulent heat fluxes during the warm and cold phases separately are also listed. Note that the positive fluxes (latent and sensible heat fluxes) are defined as heat gain by the ocean while the negative fluxes as heat loss from the ocean. As seen from Table 4, a comparison between the LHF-SST feedback and the sensible heat flux feedback indicates that the former is one order larger than the latter. Thus we only discuss the LHF-SST feedback in the following sections.

The LHF-SST feedbacks from two reference datasets, i.e. the NCEP/NCAR reanalysis and OAFlux, are comparable (about $-10Wm^{-2}K^{-1}$) during the entire ENSO cycles (Table 4). The LHF-SST feedback serves as a damper to SST change. The

LHF-SST feedbacks are poorly simulated. Nearly all models underestimate this negative feedback except for two models (CCSR MIROC_M and MRI CGCM). The overestimates of LHF-SST feedbacks in CCSR MIROC_M and MRI CGCM are within the range of estimate uncertainty. The LHT-SST feedbacks in 11 models are nearly zero or even of the opposite sign to the observation. In the cold phase, the LHF-SST feedbacks from the NCEP/NCAR reanalysis and OAFlux are about $-8.0 Wm^{-2}K^{-1}$, which are slightly weaker than those during the ENSO cycles. The model performances for the cold phase are much better than those during the ENSO cycles: most of the models obviously show negative LHF-SST feedbacks, although some of them are nearly zero. Moreover, there are 4 models (GFDL AM2p10, CCSR MIROC_M, NASA NSIPP1 and UKMO HadGAM1) having LHF-SST feedback comparable to those from NCEP/NCAR reanalysis and OAFlux. In the warm phase, the LHF-SST feedbacks from the NCEP/NCAR reanalysis and OAFlux (about $-12 Wm^{-2}K^{-1}$) are larger than those during the entire ENSO cycle. The underestimate of LHF-SST feedback in the warm phase is more outstanding. Among 16 models, only one model (CCSR MIROC_M) has a negative feedback comparable to the observations. More than half of the models have positive LHF-SST feedbacks. In particular, two models (CNRM ARPEGE3 and INM CM3) have a bias exceeding $20 Wm^{-2}K^{-1}$. These results imply that the LHF-SST feedback is another source of uncertainty among the models and these discrepancies mainly stem from the warm phase. Interestingly, in the NCEP/NCAR reanalysis and OAFlux, the LHF-SST feedback in the warm phase is slightly stronger than those in the cold phase. In the

models, the negative LHF-SST feedbacks in the warm phase are weaker than those in the clod phase.

The spatial patterns of LHF-SST feedback during the warm phase are shown in Fig. 6. The patterns from the NCEP/NCAR reanalysis and OAFlux are similar: strong negative feedback over the central-eastern tropical Pacific to the east of 140/150^{o}W and weak positive feedback over the central-western tropical Pacific to the west of date line. The negative LHF-SST feedbacks in the eastern part are well captured by all models, while the positive LHF-SST feedbacks over the western part are overestimated. Also, some models, i.e. NCAR CAM3T42, NCAR CAM3T85, CNRM ARPEGE3 and INM CM3, show excessive positive response over the climatologically intertropical convective zone region. The spatial pattern of LHF-SST feedback indicates that the discrepancy mainly stem from the bias over the central Pacific in the warm phase.

6. Summary

The extensive cold tongue problem is a long-standing tropical bias existing in the last several generations of CGCMs. Previous studies hypothesized that this excessive cold-tongue issue may be related to the weak regulating effect from the model atmosphere (Sun et al. 2003; Sun et al. 2006). Their analysis indeed shows that the regulating effect from deep convection over the underlying SST, measured by the rate of change of the net surface heat flux over the ocean, is weaker in a set of models they choose for their initial analysis. However, the two GFDL models they analyzed have a

net negative feedback that is quite close to the observation, particularly when the potential errors in the data are taken into account. In any case, whether the short length of data they used or the inclusion of La Niña episodes in their regression analysis clouds the conclusion needs to be addressed. In the present analysis, we use a much longer data set. The data from the warm phase and cold phases of ENSO are used separately for the regression analysis.

Although we start with a suspicion of the robustness of the previous results, our extended analysis further substantiates the suggestion that the excessive cold-tongue problem may have something to do with the weak regulating effect from the model atmosphere—the deep convection in particular. The analysis based on the data from the ENSO warm phase shows that all models — with no exception — have a net atmospheric feedback that is far weaker than that in the observation. While in the cold phase, some models replicate the observed $\partial Fs/\partial T$ feedback. Further more, this result underscores the relationship between the underestimate of feedbacks and deep convection. The $\partial Cs/\partial T$ feedback is found to be the major contributor to the weak $\partial Fs/\partial T$ feedback, especially in the warm phase, which is tightly related to the deep convection. In addition, a systematic feedback bias from the latent heat flux is also detected. The results underscore the potentially critical role of deep convection in the large-scale tropical ocean-atmosphere interaction, and the continuing difficulty in capturing this role in the current state-of-the-art climate models.

Acknowledgment:

This work is jointly supported by the National Basic Research Program of China (2006CB403603), the National Natural Science Foundation of China under grant Nos. **40625014**, **40221503, 40523001.** D.-Z. Sun was supported by NOAA's office of global programs and NSF Climate Dynamics Program (ATM-9912434, ATM-0331760, and ATM-0553111). Using data from the Atmospheric Model Inter-comparison Project (AMIP), this work was also partially supported under the auspices of the U.S. Dept. of Energy, Office of Science, at the University of California Lawrence Livermore National Laboratory under Contract W-7405-Eng-48.

References:

Allan, R. P., A. Slingo, and M. A. Ringer, 2002: Influence of dynamics on the changes in tropical cloud radiative forcing during the 1998 El Niño. *J. Climate*, **15**(14)**,** 1979-1986.

Barkstrom, B. R., 1984: The Earth Radiation Budget Experiment (ERBE). *Bull. Amer. Meteor. Soc.*, **65**(11)**,** 1170-1185.

Cess, R. D., M. Zhang, B. A. Wielicki, D. F. Young, X. L. Zhou, and Y. Nikitenko, 2001: The influence of the 1998 El Niño upon cloud-radiative forcing over the Pacific warm pool. *J. Climate*, **14**(9)**,** 2129-2137.

Charlock, T. P. and V. Ramanathan, 1985: The albedo field and cloud radiative forcing produced by a general circulation model with internally generated cloud optics. *J. Atmos. Sci.*, **42**(13)**,** 1408-1429.

Davey, et al., 2002: STOIC: a study of coupled model climatology and variability in tropical ocean regions. *Climate Dyn.*, **18**(5)**,** 403-420.

Feely, R.A., Wanninkhof, R., Takahashi, T. and Tans, P., 1999: Influence of El Niño on the equatorial Pacific contribution to atmospheric CO2 accumulation. *Nature*, **398**, 597-601.

Hoerling, M. P., A. Kumar, and M. Zhong, 1997: El Niño, Na Niña, and the nonlinearity of their teleconnections. *J. Climate*, **1151**(10)**,** 1769-1786.

Kistler, R. et al., 2001: The NCEP-NCAR 50-year reanalysis: monthly means CD-ROM and documentation. *Bull. Amer. Meteor. Soc.*, **82**(2)**,** 247-267.

Large, W. G. and G. Danabasoglu, 2006: Attribution and impacts of upper-ocean

biases in CCSM3. *J. Climate*, **19**(11)**,** 2325-2346.

Latif, M., et al., 2001: ENSIP: the El Niño simulation intercomparison project. *Climate Dyn.*, **18**(3)**,** 255-276.

Lin, J. L., 2007: The double-ITCZ problem in IPCC AR4 coupled GCMs: ocean-atmosphere feedback analysis. *J. Climate*, **20**(18)**,** 4497-4525.

Lin, P., H. Liu, and X. Zhang, 2008: Effect of chlorophyll-a spatial distribution on upper ocean temperature in the central and eastern equatorial Pacific. *Adv. Atmos. Sci.*, **25**(04)**,** 585-596.

Lu, R., B. Dong, R. D. Cess, and G. L. Potter, 2004: The 1997/98 El Niño: a test for climate models. *Geophys. Res. Lett.*, **31**, doi: 10.1029/2004GL019956.

Mechoso, C. R., et al., 1995: The seasonal cycle over the tropical pacific in coupled ocean-atmosphere general circulation models. *Mon. Wea. Rev.*, **123**(9)**,** 2825-2838.

Murtugudde, R., J. Beauchamp, C. R. McClain, M. Lewis, and A. J. Busalacchi, 2002: Effects of penetrative radiation on the upper tropical ocean circulation. *J. Climate*, **15**(5)**,** 470-486.

Newell, R., 1979: Climate and the ocean. *American Scientist*, **67,** 405-416.

Ramanathan, V. and W. Collins, 1991: Thermodynamic regulation of ocean warming by cirrus clouds deduced from observations of the 1987 El Niño. *Nature*, **351**(6321)**,** 27-32.

Raval, A. and V. Ramanathan, 1989: Observational determination of the greenhouse effect. *Nature*, **342,** 758-761.

Smith, T. M. and R. W. Reynolds, 2004: Improved extended reconstruction of SST (1854-1997). *J. Climate*, **17**(12)**,** 2466-2477.

Stockdale, T. N., A. J. Busalacchi, D. E. Harrison, and R. Seager, 1998: Ocean modeling for ENSO. *J. Geophys. Res.*, **103**(C7), 14,325–14,355.

Sud, Y. C., G. K. Walker, and K. M. Lau, 1999: Mechanisms regulating sea-surface temperatures and deep convection in the tropics. *Geophys. Res. Lett.*, **26**(8)**,** 1019-1022.

Sun, D. Z., 2000: The heat sources and sinks of the 1986–87 El Niño. *J. Climate*, **13**(20)**,** 3533-3550.

Sun, D.-Z., 2003: A Possible Effect of An Increase in the Warm-pool SST on the Magnitude of El Niño Warming. *J. Climate*, **16**, 185-205

Sun, D. Z. et al., 2006: Radiative and dynamical feedbacks over the equatorial cold tongue: results from nine atmospheric GCMs. *J. Climate*, **19,** 4059-4075.

Sun, D. Z., J. Fasullo, T. Zhang, and A. Roubicek, 2003: On the radiative and dynamical feedbacks over the equatorial Pacific cold tongue. *J. Climate*, **16**(14)**,** 2425-2432.

Sun, D. and K. E. Trenberth, 1998: Coordinated heat removal from the equatorial Pacific during the 1986-87 El Niño. *Geophys. Res. Lett.*, **25,** 2659-2662.

Sun, D., Y. Yu, and T. Zhang, 2008: Tropical water vapor and cloud feedbacks in climate models: a further assessment using coupled simulations. *J. Climate*. In press.

Uppala, S. M., P. W. Kallberg, A. J. Simmons, U. Andrae, V. D. C. Bechtold, M.

Fiorino, and Co-authors, 2005: The ERA-40 reanalysis. *Quart. J. Roy. Meteor. Soc.*, **131,** 2961-3012.

Wallace, J.M., 1992: Effect of deep convection on the regulation of the tropical sea surface temperature. *Nature*, **357**, 230 – 231.

Wang, C. and P. C. Fiedler, 2006: ENSO variability and the eastern tropical pacific: a review. *Progress in Oceanography*, **69**(2-4)**,** 239-266.

Weng, H., K. Ashok, S. Behera, S. Rao, and T. Yamagata, 2007: Impacts of recent El Niño Modoki on dry/wet conditions in the Pacific rim during boreal summer. *Climate Dyn.*, **29**(2)**,** 113-129.

Wittenberg, A. T., A. Rosati, N. C. Lau, and J. J. Ploshay, 2006: GFDL's CM2 global coupled climate models. Part iii: tropical pacific climate and ENSO. *J. Climate*, **19**(5)**,** 698-722.

Wu, F., H. Liu, W. Li, and X. Zhang, 2005: Effects of adjusting vertical resolution on the eastern equatorial Pacific cold tongue. *Acta Oceanologica Sinica*, **24**(3)**,** 1 – 12.

Yu, L. and R. A. Weller, 2007: Objectively analyzed air-sea heat fluxes for the global ice-free oceans (1981-2005). *Bull. Amer. Meteor. Soc.*, **88**(4)**,** 527-539.

Yu, L., X. Jin, and R. A. Weller, 2006: Role of net surface heat flux in seasonal variations of sea surface temperature in the tropical Atlantic ocean. *J. Climate*, **19**(23)**,** 6153-6169.

Zhang, G. J. and M. J. McPhaden, 1995: The relationship between sea surface temperature and latent heat flux in the equatorial Pacific. *J. Climate*, **8**(3)**,**

589-605.

Zhang, Y., W. B. Rossow, A. A. Lacis, V. Oinas, and M. I. Mishchenko, 2004: Calculation of radiative fluxes from the surface to top of atmosphere based on ISCCP and other global data sets: refinements of the radiative transfer model and the input data. *J. Geophys. Res.*, **109**(D19105), doi: 1029/2003JD004457.

Table 1 Descriptions list of models that participated in this study.

Institute	AGCM	Resolution	Name used for discussion
NCAR	CAM2	T42 L26	NCAR CAM2
NCAR	CAM3	T42 L26	NCAR CAM3T2
NCAR	CAM3	T85 L26	NCAR CAM3T85
IAP	GAMIL1.0	2.8 x 2.8 L26	IAP GAMIL1
GFDL	AM2p10	2.5 x 2.0 L18	GFDL AM2p10
GFDL	AM2p12	2.5 x 2.0 L24	GFDL AM2p12
CCSR	MIROC3_2(medres)	T42 L20	CCSR MIROC_H
CCSR	MIROC3_2(hires)	T106 L56	CCSR MIROC_M
MRI	-	T42 L30	MRI CGCM
NASA/GISS	-	4.0 x 5.0 L20	NASA GISS_ER
NASA	NSIPP1	2.5 x 2.0 L34	NASA

			NSIPP1
UKMO	**HadGAM1**	**N96 L38**	**UKMO HadGAM1**
MPI	**ECHAM5**	**T63 L32**	**MPI ECHAM5**
IPSL	**LMDZ4**	**2.5 x 3.75 L19**	**IPSL LMDZ4**
CNRM	**ARPEGE3**	**T42 L45**	**CNRM ARPEGE3**
INM	**-**	**4.0x5.0 L21**	**INM CM3**

Table 2 Atmospheric feedbacks over the equatorial Pacific cold tongue region (5^oS~5^oN, 150^oE~110^oW) estimated from observation and models over the period of 1985 through 1999 during the entire ENSO cycle. Numbers in parenthesis are estimates from the NCEP/NCAR reanalysis. Unit is $Wm^{-2}K^{-1}$.

IPCC ID	∂Ga/∂T	∂Cl/∂T	∂Cs/∂T	∂Da/∂T	∂Fa/∂T	∂Fs/∂T
ISCCP\ OAFlux	7.03±0.25	12.55±0.66	-13.98±0.83	-21.21±1.26 (-20.56±1.69)	-15.10±1.22	-21.51±1.26 (-19.69±1.67)
NCAR CAM2	8.92±0.24	8.78±0.44	2.43±0.55	-12.53±0.89	7.60±0.84	1.80±0.81
NCAR CAM3T2	9.35±0.24	8.37±0.45	-0.47±0.63	-11.14±0.87	6.11±0.89	0.06±0.90
NCAR CAM3T85	9.96±0.24	12.72±0.66	-10.36±0.80	-15.41±1.09	-3.09±1.14	-9.18±1.14
IAP GAMIL1	7.87±0.16	9.18±0.42	-4.44±0.39	-12.02±0.83	0.60±0.76	-5.47±0.76
GFDL AM2p10	8.93±0.23	14.99±0.55	-14.01±0.63	-16.92±0.87	-7.02±0.93	-12.97±0.93
GFDL AM2p12	10.01±0.23	17.31±0.74	-14.65±0.86	-21.04±1.19	-8.38±1.28	-14.40±1.28
CCSR MIROC_H	8.13±0.19	10.57±0.50	-2.68±0.50	-19.58±0.93	-3.56±0.86	-9.65±0.87
CCSR MIROC_M	7.26±0.16	12.27±0.47	-3.58±0.47	-27.42±1.00	-11.47±0.96	-17.39±0.97
MRI CGCM	9.43±0.26	13.32±0.63	-5.45±1.11	-28.73±1.37	-11.43±1.45	-17.53±1.46
NASA GISS_ER	7.35±0.30	9.34±0.47	-7.86±0.50	-13.73±0.86	-4.85±0.83	-9.79±0.87
NASA NSIPP1	9.67±0.22	13.44±0.52	-11.36±0.60	-20.47±0.85	-8.72±0.87	-14.73±0.87
UKMO HadGAM1	10.89±0.41	13.90±0.74	-13.01±0.82	-22.68±1.16	-10.90±1.21	-16.73±1.21
MPI ECHAM5	10.28±0.28	17.34±0.72	-19.90±1.08	-26.39±1.30	-18.66±1.57	-24.36±1.57
IPSL LMDZ4	9.67±0.22	17.04±0.70	-15.18±0.83	-20.70±0.95	-9.18±0.89	-15.13±0.89
CNRM ARPEGE3	9.09±0.26	12.61±0.67	-13.91±0.73	-10.13±1.28	-2.35±1.14	-7.38±1.14
INM CM3	10.39±0.34	16.53±1.00	-17.21±1.36	-14.64±1.08	-4.93±1.20	-10.95±1.21

Table 3 Same as for Table 2, but for the warm phase condition. Unit is $Wm^{-2}K^{-1}$.

IPCC ID	∂Ga/∂T	∂Cl/∂T	∂Cs/∂T	∂Da/∂T	∂Fa/∂T	∂Fs/∂T
ISCCP\ OAFlux	9.98±0.69	16.78±1.67	-23.56±2.29	-22.84±2.95 (-21.44±2.59)	-19.65±2.94	-26.29±2.99 (-22.78±1.81)
NCAR CAM2	11.38±0.55	12.73±1.15	3.25±1.43	-13.64±2.35	13.72±2.22	8.02±2.13
NCAR CAM3T2	11.70±0.47	10.91±1.15	-1.83±1.48	-10.30±2.36	10.48±2.43	4.43±2.44
NCAR CAM3T85	11.89±0.55	13.42±1.79	-14.58±2.24	-14.39±3.08	-3.66±3.34	-9.78±3.35
IAP GAMIL1	9.28±0.34	10.02±1.08	-4.63±1.01	-7.58±2.14	7.09±2.00	1.03±2.00
GFDL AM2p10	10.94±0.44	18.93±1.38	-18.83±1.50	-14.31±2.38	-3.27±2.56	-9.20±2.56
GFDL AM2p12	12.22±0.47	23.23±1.81	-22.05±2.17	-20.05±3.26	-6.65±3.55	-12.67±3.55
CCSR MIROC_H	10.21±0.41	14.83±1.22	-6.20±1.23	-21.84±2.41	-2.99±2.30	-9.29±2.34
CCSR MIROC_M	7.77±0.38	13.83±1.27	-4.21±1.21	-27.54±2.49	-10.14±2.40	-16.03±2.43
MRI CGCM	11.65±0.55	16.45±1.57	-11.06±2.84	-23.86±3.38	-6.82±3.92	-13.05±3.94
NASA GISS_ER	9.07±0.79	12.31±1.29	-10.77±1.35	-14.24±2.42	-3.56±2.26	-9.05±2.46
NASA NSIPP1	12.60±0.48	19.65±1.28	-18.06±1.47	-20.67±2.32	-6.48±2.40	-12.49±2.41
UKMO HadGAM1	15.19±0.97	20.05±1.93	-19.18±2.10	-27.04±3.15	-10.99±3.23	-16.79±3.24
MPI ECHAM5	11.91±0.62	19.36±1.84	-23.03±2.90	-24.53±3.26	-16.29±4.19	-21.90±4.21
IPSL LMDZ4	11.66±0.48	19.47±1.85	-22.18±2.09	-18.32±2.44	-9.37±2.39	-15.25±2.39
CNRM ARPEGE3	10.81±0.65	14.49±1.69	-17.20±1.81	-5.39±3.34	2.71±3.04	-2.22±3.03
INM CM3	13.35±0.83	25.56±2.72	-29.81±3.67	-14.35±2.99	-5.25±3.44	-11.45±3.47

Table 4 The feedback from the latent heat flux (hfls) and sensible heat flux (hfss) for the entire ENSO cycle, the cold phase, and the warm phase. Unit is $Wm^{-2}K^{-1}$.

Model ID	Total SST		Cold phase		Warm phase	
	hfls	hfss	hfls	hfss	hfls	hfss
NCEP1	-10.46±0.84	-1.89±0.10	-7.27±1.59	-1.54±0.19	-12.21±2.23	-0.22±0.26
OAFlux	-9.40±0.57	-1.82±0.08	-8.46±1.19	-1.34±0.14	-10.49±1.45	-0.12±0.23
NCAR CAM2	-0.86±0.61	-0.80±0.07	-3.42±1.25	-0.82±0.16	2.66±1.55	-0.63±0.18
NCAR CAM3T2	1.58±0.64	-0.99±0.08	-1.54±1.36	-0.38±0.19	5.95±1.54	-0.28±0.17
NCAR CAM3T85	0.32±0.62	-0.42±0.08	-0.24±1.26	0.38±0.19	2.65±1.64	-0.91±0.17
IAP GAMIL1	-1.13±0.64	-0.71±0.05	-6.66±1.15	-0.73±0.12	4.40±1.59	-0.46±0.12
GFDL AM2p10	-2.08±0.84	1.07±0.09	-8.50±1.42	0.69±0.21	4.46±2.16	1.66±0.19
GFDL AM2p12	-2.09±0.90	0.71±0.07	-6.24±1.66	0.54±0.14	4.57±2.34	1.43±0.14
CCSR MIROC_H	-4.08±0.60	-0.39±0.05	-4.41±1.21	-0.15±0.10	-0.85±1.54	-0.27±0.12
CCSR MIROC_M	-10.94±0.65	-0.97±0.05	-10.60±1.54	-0.68±0.11	-9.20±1.51	-1.01±0.13
MRI CGCM	-12.72±1.02	1.42±0.19	-15.27±2.22	1.11±0.36	-5.87±2.43	2.92±0.50
NASA GISS_ER	0.85±0.71	0.20±0.07	-2.99±1.38	-0.01±0.15	4.15±1.85	0.86±0.18
NASA NSIPP1	-7.05±0.60	1.70±0.09	-8.56±1.10	1.16±0.16	-1.54±1.59	2.75±0.22
UKMO HadGAM1	-5.78±0.96	-0.53±0.06	-9.68±1.98	-0.48±0.12	-1.45±2.44	-0.64±0.14
MPI ECHAM5	-5.89±0.93	-1.24±0.10	-7.29±2.04	-0.94±0.21	-2.04±2.28	-0.85±0.25
IPSL LMDZ4	0.47±0.57	-0.49±0.08	-3.93±1.18	-1.00±0.15	4.25±1.31	0.29±0.18
CNRM ARPEGE3	4.75±0.85	0.95±0.06	-0.20±1.55	0.78±0.14	13.27±2.12	0.86±0.15
INM CM3	3.44±0.84	1.24±0.14	-0.69±1.52	1.18±0.30	12.04±2.10	2.31±0.34

Figure captions

Fig. 1. Shown are the time series of SST (Left y-coordinate, solid line) and SST anomaly (Right y-coordinate, dashed line) averaged over the Pacific cold-tongue region (5^oS~5^oN, 150^oE~110^oW). The red (blue) part of the solid line is the SST during the warm (cold) phase. The warm (cold) phase is defined by the sign of SST anomaly averaged over the Pacific cold-tongue region (dashed line).

Fig. 2. Response of the net surface heat flux (Fs) in observations and models to an increase in the cold-tongue SST. Shown are the results obtained for the entire ENSO cycle. Positive fluxes indicate heat gain by the ocean, while negative fluxes indicate heat loss from the ocean. Shown are regression coefficients obtained by linearly regressing the Fs against the SST anomaly averaged over the Pacific cold tongue region (5^oS~5^oN, 150^oE~110^oW). The interannual variations from 1985 to 1999 are used for the calculation. Unit is $Wm^{-2}K^{-1}$.

Fig. 3. Same as Fig. 2., but for the response of cloud shortwave radiative forcing (Cs).

Fig. 4. Differences in the response of Fs to an increase in the cold-tongue SST between the warm phase situation and the whole ENSO cycle situation. Positive fluxes indicate heat gain by the ocean, while negative fluxes indicate heat loss from the ocean. Shown are the differences in the regression coefficients between the two situations. The regression coefficients are obtained by linearly regressing Fs against the SST averaged over the Pacific cold tongue region (5^oS~5^oN, 150^oE~110^oW). The interannual variations during 1985 to 1999 are used for the calculation. Unit is $Wm^{-2}K^{-1}$.

Fig. 5. Same as Fig. 4., but for the differences in the response of Cs.

Fig. 6. Spatial patterns of latent heat flux response to an increase in the cold-tongue SST for the warm phase situation. Positive fluxes indicate heat gain by the ocean, while negative fluxes indicate heat loss from the ocean. Shown are regression coefficients from observations and models. The regression

coefficients are obtained by linearly regressing the latent heat flux against the SST averaged over the Pacific cold-tongue region (5^oS~5^oN, 150^oE~110^oW). The interannual variations from 1985 to 1999 are used for the calculation. Unit is $Wm^{-2}K^{-1}$.

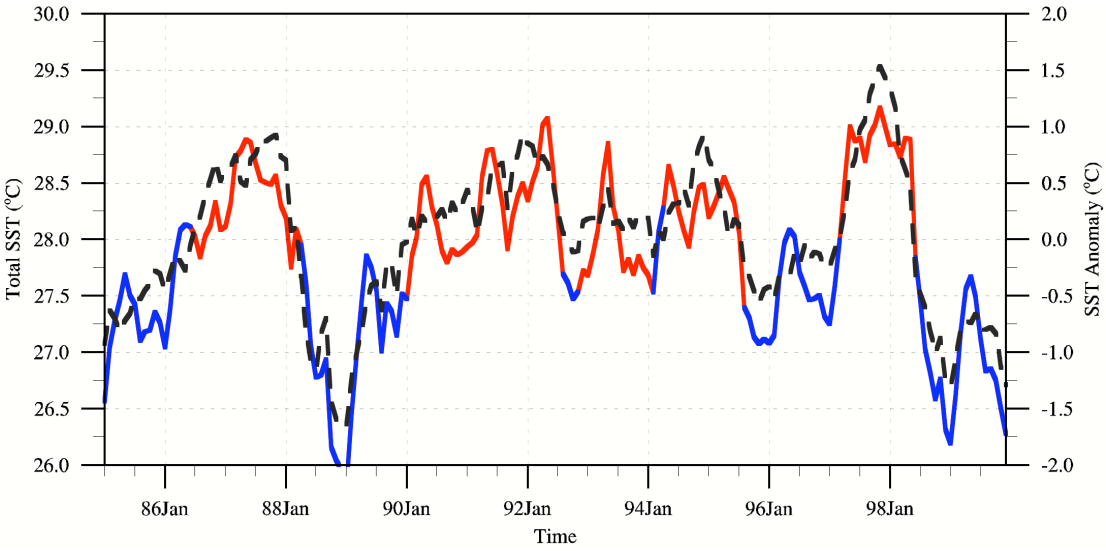

Fig. 1. Shown are the time series of SST (Left y-coordinate, solid line) and SST anomaly (Right y-coordinate, dashed line) averaged over the Pacific cold-tongue region (5°S~5°N, 150°E~110°W). The red (blue) part of the solid line is the total SST during the warm (cold) phase. The warm (cold) phase is defined by the sign of SST anomaly averaged over the Pacific cold-tongue region (dashed line).

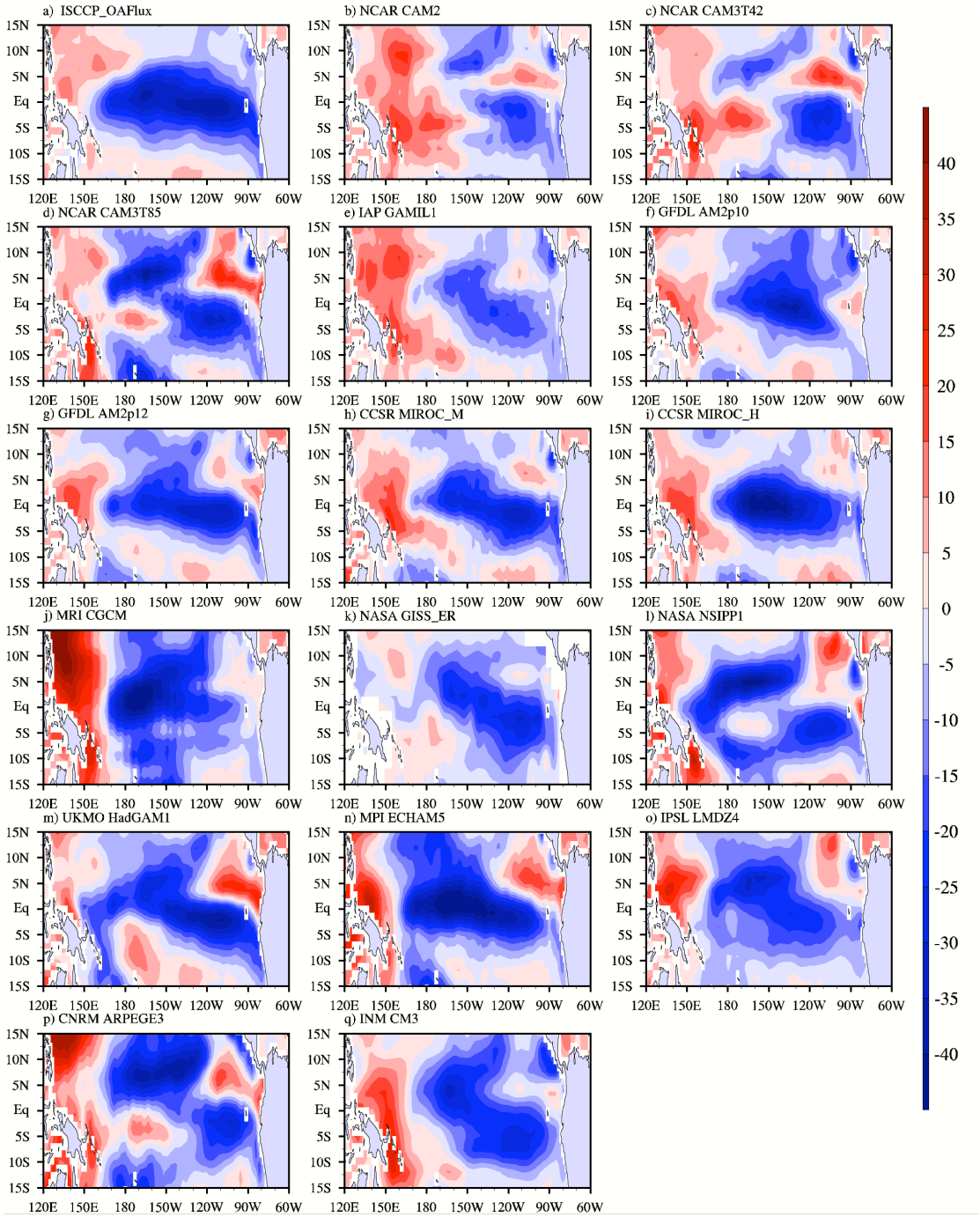

Fig. 2. Response of the net surface heat flux (Fs) in observations and models to an increase in the cold-tongue SST. Shown are the results obtained for the entire ENSO cycle. Positive fluxes indicate heat gain by the ocean, while negative fluxes indicate heat loss from the ocean. Shown are regression coefficients obtained by linearly regressing the Fs against the SST anomaly averaged over the Pacific cold tongue region (5^{o}S~5^{o}N, 150^{o}E~110^{o}W). The interannual variations from 1985 to 1999 are used for the calculation. Unit is $Wm^{-2}K^{-1}$.

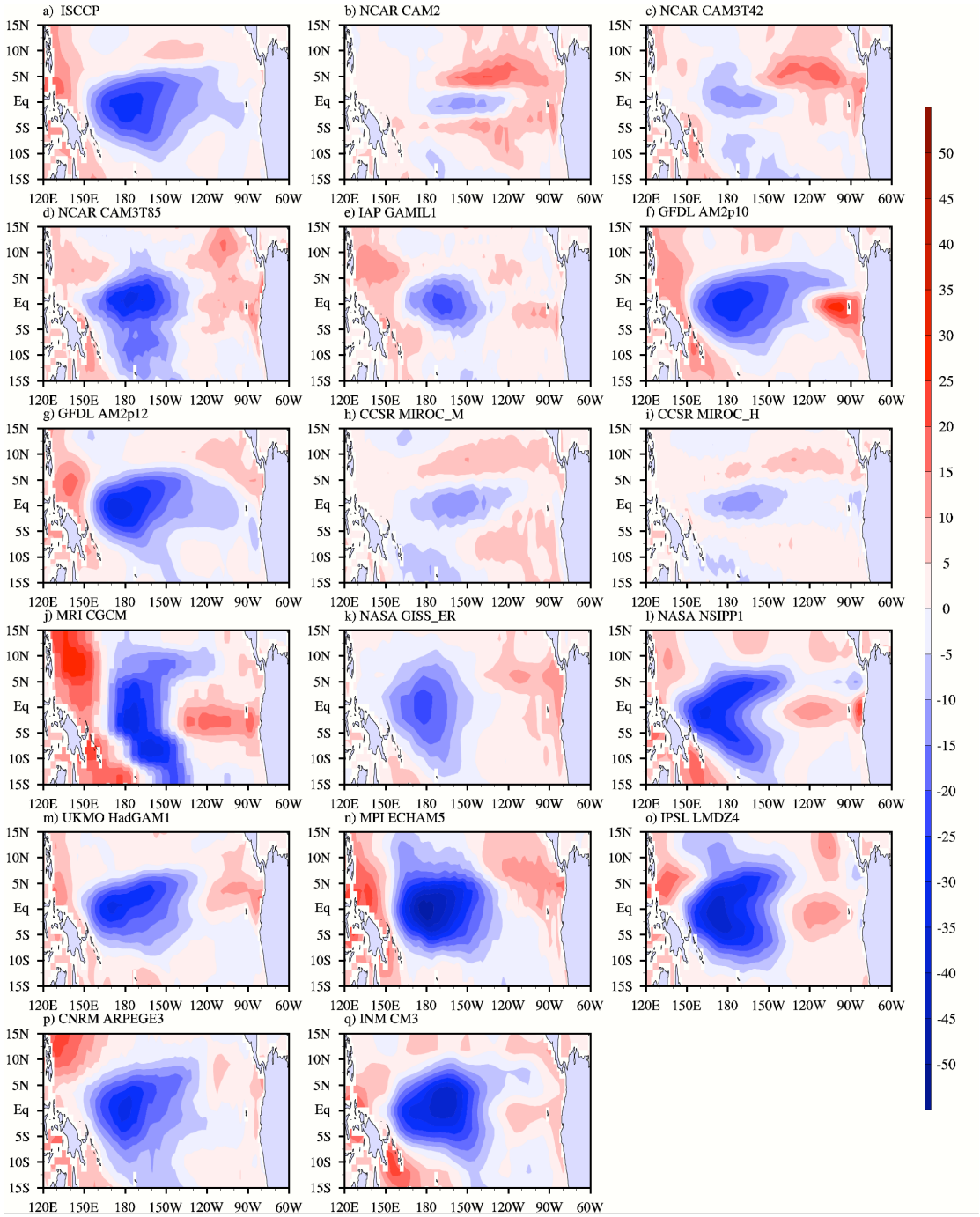

Fig. 3. Same as Fig. 2., but for the response of cloud shortwave radiative forcing (Cs).

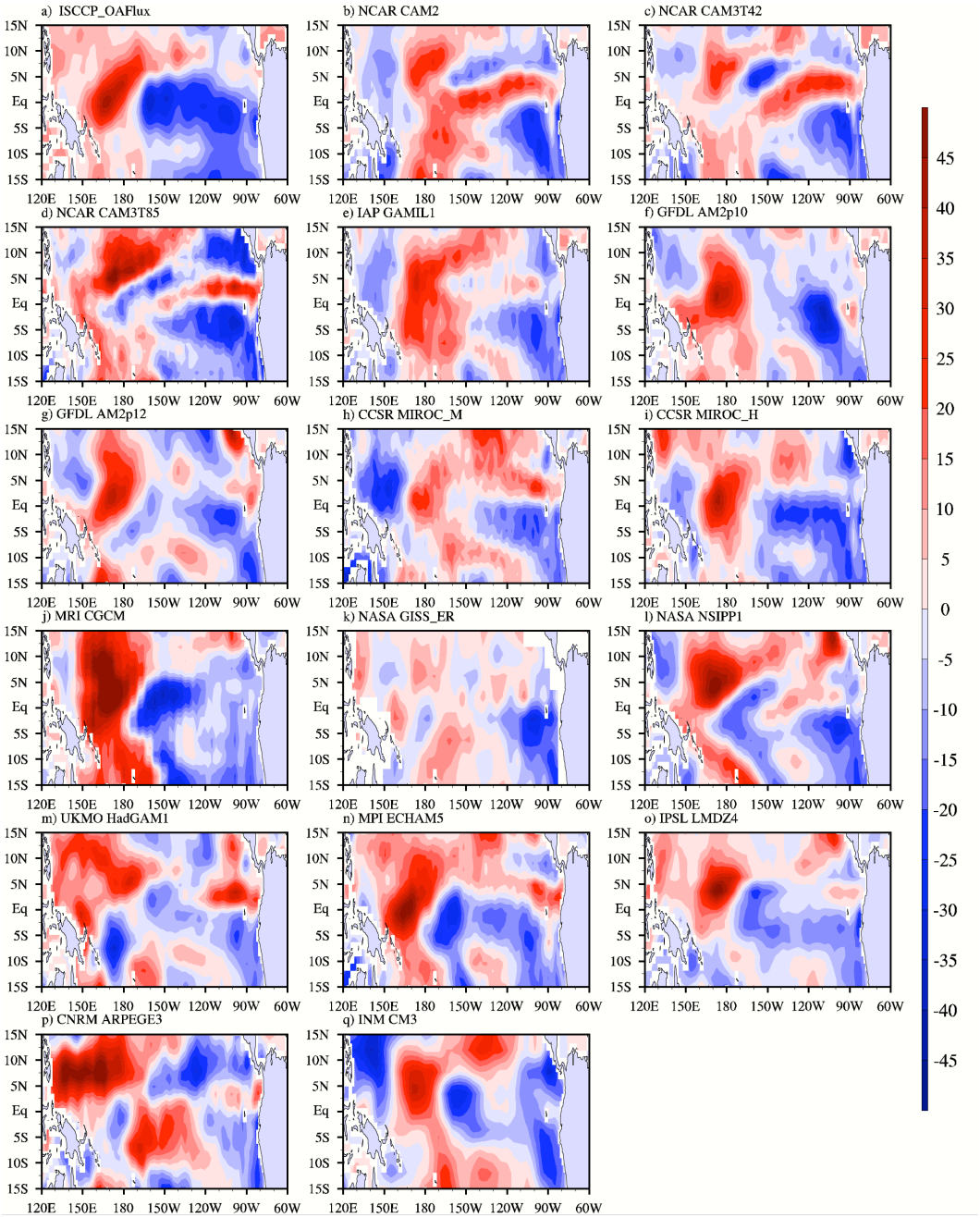

Fig. 4. Differences in the response of Fs to an increase in the cold-tongue SST between the warm phase situation and the whole ENSO cycle situation. Positive fluxes indicate heat gain by the ocean, while negative fluxes indicate heat loss from the ocean. Shown are the differences in the regression coefficients between the two situations. The regression coefficients are obtained by linearly regressing Fs against the SST averaged over the Pacific cold tongue region (5^{o}S~5^{o}N, 150^{o}E~110^{o}W). The interannual variations during 1985 to 1999 are used for the calculation. Unit is $Wm^{-2}K^{-1}$.

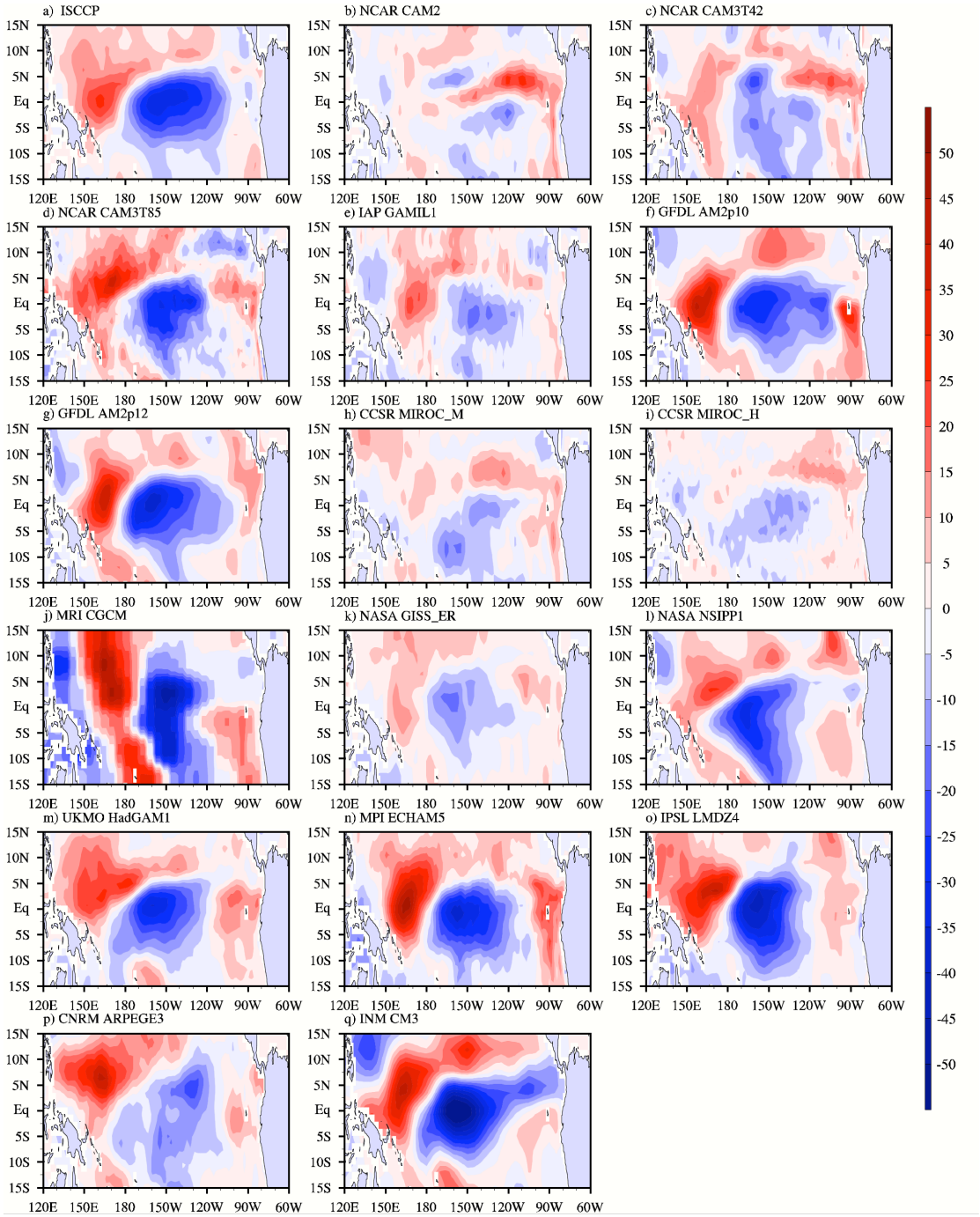

Fig. 5. Same as Fig. 4., but the difference maps for the response of the Cs.

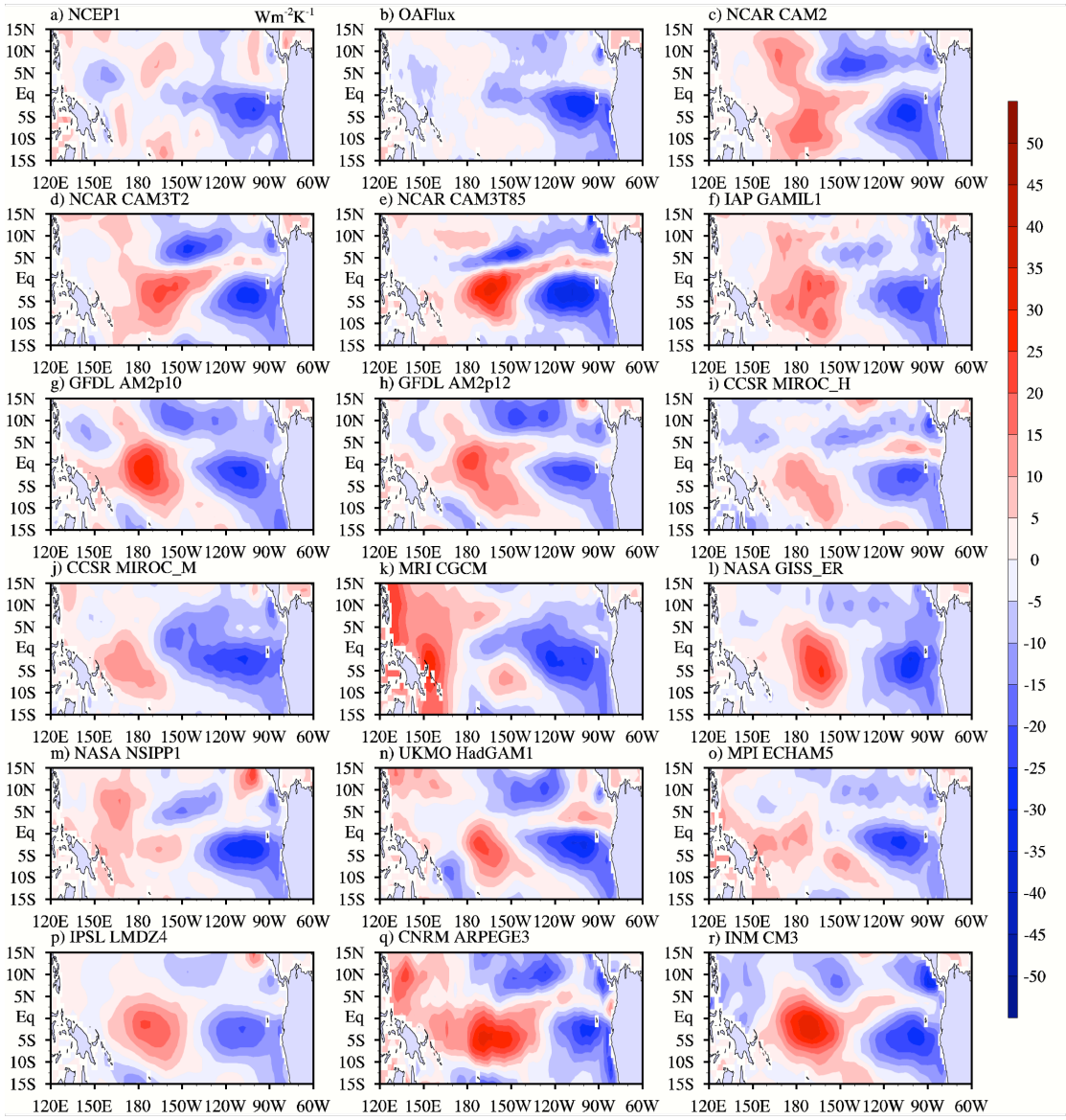

Fig. 6. Spatial patterns of latent heat flux response to an increase in the cold-tongue SST for the warm phase situation. Positive fluxes indicate heat gain by the ocean, while negative fluxes indicate heat loss from the ocean. Shown are regression coefficients from observations and models. The regression coefficients are obtained by linearly regressing the latent heat flux against the SST averaged over the Pacific cold-tongue region (5°S~5°N, 150°E~110°W). The interannual variations from 1985 to 1999 are used for the calculation. Unit is $Wm^{-2}K^{-1}$.